Sound propagation in liquid water: The puzzle continues

Francesco Sciortino
CRS4, Centro di Ricerca, Sviluppo e Studi Superiori in Sardegna, P. O. Box 488, 09100, Cagliari, Italy and Dipartimento di Fisica, Universitá di Roma "La Sapienza," Piazzale Aldo Moro, 00185 Rome, Italy

Srikanth Sastry[a]
Center for Polymer Studies and Department of Physics, Boston University, Boston, Massachusetts 02215

Experimental and simulation studies of sound propagation in water have observed, at large wave vectors k ($k > 0.25$ Å^{-1}), a longitudinal sound mode with a velocity of about 3500 m/s, more than twice the hydrodynamic sound velocity. The relation between the hydrodynamic sound mode and the high frequency mode has been the center of contrasting interpretations. In this paper, we report extensive molecular dynamics simulations designed *ad hoc* to explore the intermediate and low k part of the collective spectrum. We calculate the dispersion relations for longitudinal and transverse collective modes from 0.026 to 1 Å^{-1} for a range of temperatures. At all temperatures studied, the sound velocity increases with k. At the highest studied temperature, the sound velocity changes from values comparable to hydrodynamic sound velocity to ones observed by neutron scattering experiments. We show that the viscoelastic approximation describes the data satisfactorily. We also perform normal mode analysis of quenched liquid configurations to obtain further information about the behavior observed at intermediate frequencies (50–100 cm^{-1}). We find further positive dispersion of the sound branch at these frequencies and indications which suggest the interaction of the sound branch with localized modes as the origin of such dispersion.

I. INTRODUCTION

The propagation of the sound in liquid water has received a lot of attention in recent years.[1-5] In particular, the dispersion relation at large wave vector k has been the subject of contrasting interpretations and is still a controversial topic. In the region of $k > 0.25$ Å^{-1}, both experiments and simulations observe a sound mode with a velocity of about 3500 m/s, a velocity more than twice the hydrodynamic sound velocity.

It has been suggested that this high frequency mode is a manifestation of collective excitations in patches of hydrogen bonded molecules.[1] According to this interpretation, such excitations are distinct from the collective excitations observed at low frequencies and thus constitute a novel phenomenon arising from the hydrogen bonded network topology in liquid water. The ordinary sound mode is not observed in this region due to increased damping on increasing the frequency. The similarity in the values of the high k sound velocity and the sound velocity in ice has been offered as supporting evidence for this interpretation.

An alternative interpretation has been proposed based on generalized hydrodynamic theory.[2,6,7] In this interpretation, the behavior seen in water can be understood within the framework developed for normal liquids. The high sound velocity observed is seen as the result of a continuous positive dispersion in the region that is not observable either by neutron or by light scattering. The behavior of the system changes smoothly from the one characteristic of viscous fluids to that of elastic materials. According to this interpretation, there is at most one sound peak in the dynamic structure factor, with a damping related to the magnitude of the dispersion. The change by a factor of 2 in the value of the sound velocity in going from the hydrodynamic regime to $k > 0.25$ Å^{-1} that is seen in water is unusual, but can be related to the peculiar interaction between water molecules, the hydrogen bonds. Support for this interpretation comes from the extrapolation to intermediate k of data extracted by molecular dynamics (MD) simulations.

The two interpretations predict a completely different behavior in the region not accessible to experiments. The wavelengths of light and of neutrons do not allow direct observation in the relevant part of the (ω, k) plane.

MD simulations have been a powerful tool for analyzing collective excitations. In fact, the high frequency mode was observed first in a MD simulation with the ST2[8] potential and was confirmed by experiments only a few years later. One expects that the previously described interpretations could be tested by MD simulations with some representative potential. Such efforts have been limited by the difficulty of simulating large systems (i.e., small k) for very long times (i.e., low frequencies). Previous MD simulations with up to 500 molecules have confirmed the capability of many model potentials to reproduce the experimental high velocity branch, but have not been able to distinguish convincingly between the two interpretations.[2-4,8,9]

In this paper, we describe an extensive set of MD simulations designed *ad hoc* to explore the low k part of the collective spectrum. We calculate longitudinal and trans-

verse collective modes in the range 0.026 to 1 Å^{-1}, a range extending to k values more than ten times smaller than previously reported analyses. By studying a rectangular box containing 2988 water molecules at five different temperatures for times of about 400 ps each, we are able to cover the region where the sound velocity changes. To obtain more information about behavior observed at intermediate frequencies (50–100 cm^{-1}; 1 cm^{-1}=0.03 THz =0.1885 ps^{-1}), we also perform normal mode analysis of quenched liquid configurations.

The results we obtain suggest that the viscoelastic approximation (VA) describes the transverse collective excitations very well, excitations whose peaks are confined below 50 cm^{-1}. The collective longitudinal excitations are also well described by the viscoelastic approximation for small k, when the propagation peaks are again below 50 cm^{-1}. Between 50 and 100 cm^{-1}, the frequency range in which the O–O–O bending mode has previously been reported,[5] normal mode analysis of quenched configurations suggests that localized modes present in the liquid may produce additional dispersion and be relevant to understanding sound propagation in this frequency range.

II. COMPUTATION DETAILS AND DEFINITIONS

Simulations are performed at five different temperatures for a system composed of 2988 molecules in a rectangular box of dimension $234 \times 19.5 \times 19.5$ Å. The density is fixed at 0.998 g/cm^3 for all the simulations. Molecules interact via the TIP4P potential,[10] a two body rigid model that was previously used to study the region with $k > 0.3$ Å^{-1}.[3] Simulations were performed in the constant number of molecules, volume, and energy (NVE) ensemble. The integration time step was 1 fs and the reaction field technique was applied to take long range interactions into account. For each temperature, two or three simulations were performed to improve the statistical accuracy. After the equilibration period, configurations were saved on disk every 0.075 ps. This time interval fixes the upper limit on the frequencies that can be studied and is chosen as a compromise between the need of storing velocities and coordinates of the molecules and the need of performing long (up to 400 ps) simulations. The memory required to save about 300 ps with a 0.075 ps interval between configurations is about 1 GB, the size of the hard disk mounted on the IBM 590 RISC 6000 workstation on which these simulations were performed. Each run required about two months of central processing unit (CPU) time.

The collective properties are most conveniently studied in terms of Fourier components of the density and current correlation functions.[11,12] In a system with N molecules, the number density ρ and the current j at time t are given by

$$\rho(\mathbf{r},t) = \frac{1}{\sqrt{N}} \sum_{i=1,N} \delta[\mathbf{r}-\mathbf{r}_i(t)], \quad (2.1)$$

$$\mathbf{j}(\mathbf{r},t) = \frac{1}{\sqrt{N}} \sum_{i=1,N} \mathbf{v}_i(t)\delta[\mathbf{r}-\mathbf{r}_i(t)], \quad (2.2)$$

where $\mathbf{r}_i(t)$ and $\mathbf{v}_i(t)$ are the center of mass (c.m.) position and the velocity of molecule i and the subscript α indicates the Cartesian components of $\mathbf{j}_k$ and $\mathbf{v}_i$. The corresponding Fourier transforms are

$$n_\mathbf{k}(t) = \frac{1}{\sqrt{N}} \sum_{i=1,N} e^{i\mathbf{k}\cdot\mathbf{r}_i(t)}, \quad (2.3)$$

$$j_{\mathbf{k}\alpha}(t) = \frac{1}{\sqrt{N}} \sum_{i=1,N} v_{i\alpha}(t)e^{i\mathbf{k}\cdot\mathbf{r}_i(t)}. \quad (2.4)$$

The power spectrum of $n_\mathbf{k}(t)$,

$$S(\mathbf{k},\omega) = \langle |n_\mathbf{k}(\omega)|^2 \rangle, \quad (2.5)$$

is the dynamic structure factor, the quantity most commonly reported in neutron and light scattering experiments, as it is proportional to the measured differential scattering cross section. The integral over ω of $S(k,\omega)$ gives the static structure factor $S(k)$, which in the limit for $k \to 0$ yields the isothermal compressibility. From the frequency spectra of $j_{k\alpha}$ and $j_{k\beta}$ one defines

$$J_{\alpha\beta}(\mathbf{k},\omega) = \langle |j_{\mathbf{k}\alpha}^*(\omega)j_{\mathbf{k}\beta}(\omega)| \rangle. \quad (2.6)$$

From $J_{\alpha\beta}(\mathbf{k},\omega)$, the longitudinal J_l and a transverse J_t current correlation functions are obtained using

$$J_{\alpha\beta} = \frac{k_\alpha k_\beta}{k^2} J_l(k,\omega) + \left(\delta_{\alpha\beta} - \frac{k_\alpha k_\beta}{k^2}\right) J_t(k,\omega). \quad (2.7)$$

The longitudinal component $J_l(k,\omega)$ is related to $S(k,\omega)$ via the rigorous expression

$$J_l(k,\omega) = \omega^2 S(k,\omega)/k^2. \quad (2.8)$$

The transverse current gives information about the transverse collective excitations. In a viscous liquid, the transverse current fluctuations will dissipate through diffusive processes [i.e., a single peak centered at $\omega=0$ in $J_t(k,\omega)$], the rate of dissipation being governed by the shear viscosity coefficient. In viscoelastic fluids, the onset of elastic behavior at large k is associated with the appearance of peaks at finite ω values in the transverse current power spectrum.

The data presented in this article are obtained by calculating the longitudinal and transverse components of $j_{k\alpha}(t)$, i.e., with α parallel and orthogonal to k, directly from the MD trajectories. Then the power spectrum of the selected quantities is evaluated numerically using the maximum entropy method.[13] To ensure that the features observed are not spurious, these spectra are studied in conjunction with straightforward calculations using the Wiener–Khinchin theorem. Spherical k averages have been used, where possible, to improve the quality of the data.

III. THERMODYNAMIC DATA

In this section, we report some basic bulk quantities calculated from the MD trajectories. Such a comparison with available experimental data allows a better framing (in the P–T plane) of the simulated data.

In Fig. 1, the simulated data (+'s) are compared with the corresponding values (full lines) as given by the Haar, Gallagher, and Kell (HGK) equation of state.[14] In Fig.
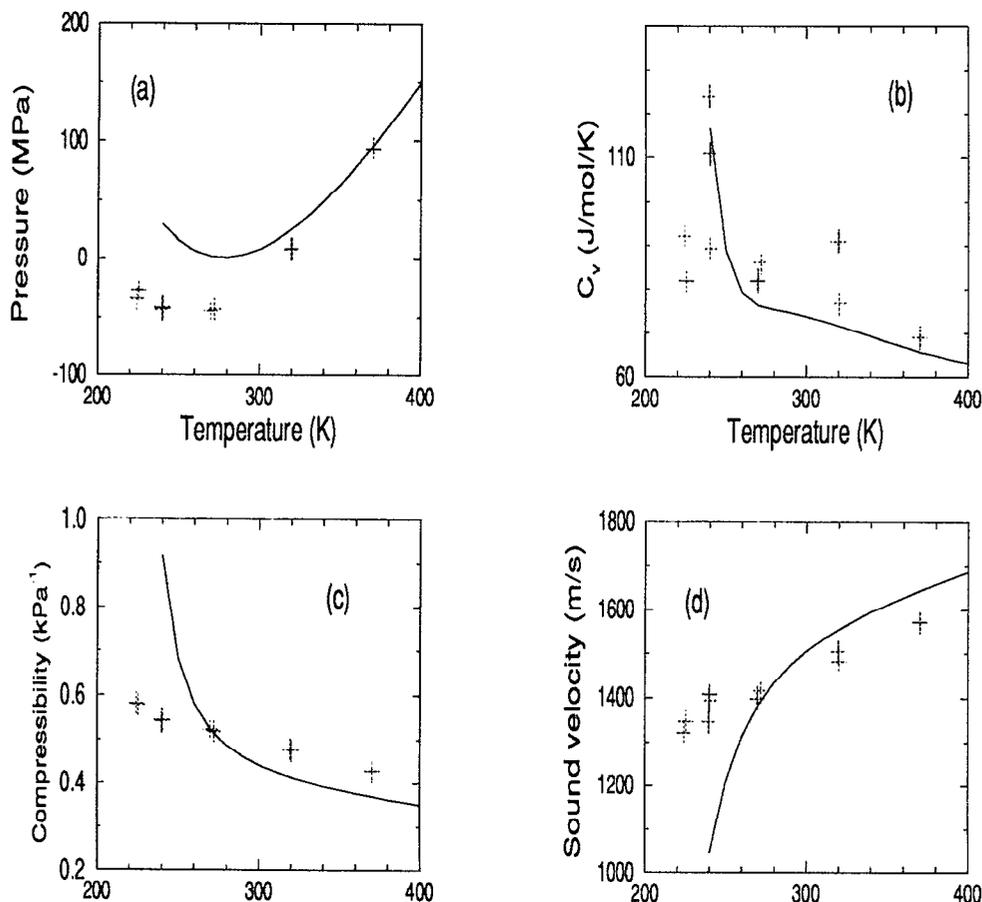
FIG. 1. A comparison of thermodynamic quantities obtained from the TIP4P simulation with values from the HGK equation of state at a constant density of 1 g/cm^3. The simulation data are represented by +'s, while the HGK values are shown as continuous lines. (a) Pressure along the isochore; (b) the constant volume specific heat; (c) the isothermal compressibility; and (d) the hydrodynamic sound velocity.

1(a), the temperature dependence of the pressure P is shown. Interestingly enough, the TIP4P potential does show a temperature of maximum density (TMD) [or a minimum of $P(T)$ along an isochore] around $T=250$ K, about 27° below the experimental minimum. The increase in P for temperatures higher than the TMD is related to the increased probability for molecules to probe the repulsive part of the potential due to increased kinetic energy. The increase in P for temperatures lower than the TMD is instead due to the progressive formation of strong linear hydrogen bonds (HBs) and the formation of regions of tetrahedrally coordinated molecules with low local density.[15] In Fig. 1(b), the temperature dependence of the constant volume specific heat C_v is shown (calculated according to Ref. 16). In Fig. 1(c), the temperature dependence of the isothermal compressibility κ_T is shown, calculated from the low k limit of the structure factor. Note that the simulation data (as well as the HGK values) do not show the well-known minimum of κ_T at 46 °C since our simulations are performed at constant volume and *not* constant pressure. In the range investigated, κ_T along an isochore is a monotonic function of temperature, increasing with decreasing temperature. Last, in Fig. 1(d), the adiabatic sound speed obtained from the combination of κ_T,

C_v, and the thermal pressure coefficient $\gamma_v\{\equiv(\partial P/\partial T)_V\}$ is shown. The calculation of γ_v and C_v by fitting the temperature dependence of the pressure and the total energy are consistent with the values obtained from the analysis of the corresponding fluctuations. The simulation values for the sound velocity show the correct (qualitative) temperature dependence.

For all the quantities shown in Fig. 1, a qualitative agreement with the corresponding experimental quantities is observed, but with a less pronounced change on supercooling. Indeed, while in real water the structuring of the HB network overcomes the normal thermal expansion below 4 °C (as evidenced by the decrease of density on cooling), in TIP4P, such equilibrium is found at about −23 °C. Moreover, the curvature of the P-T isochore on the low T side and the amount of increase in compressibility on lowering the temperature show that *anomalous behavior* is underestimated in TIP4P. As a first approximation, the existence of the temperature shift has to be taken into account in comparing experimental and calculated data, in particular, if the comparison involves quantities related to the underlying HB network.[17] If the temperature axis for the simulation data is shifted so that the simulation TMD coincides with the experimental TMD [see Fig. 1(a)], con-
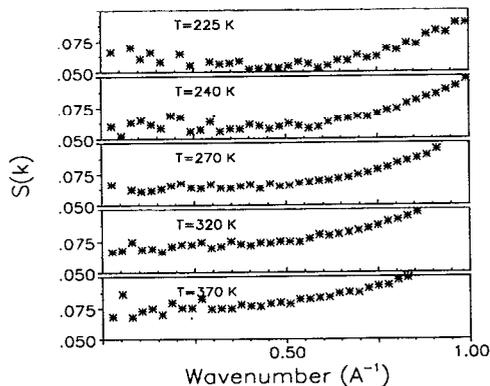
FIG. 2. The static structure factor measured from the TIP4P simulations. The temperature values are shown on the graphs.
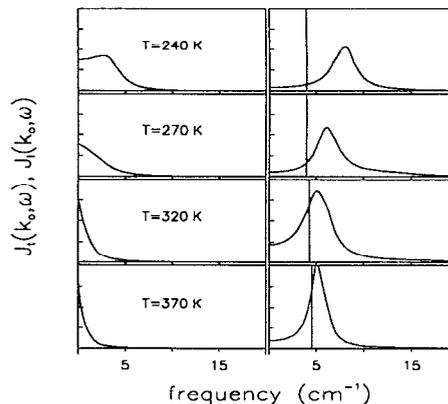

FIG. 3. Transverse and longitudinal current correlation functions $J_t(k,\omega)$ and $J_l(k,\omega)$ for various temperatures at a low k value $k_0=0.0537$ Å^{-1}. J_t's are shown in the left column and J_l's are shown in the right column. The vertical lines in the right column indicate the position of the peak expected if there is no positive dispersion, given by the product of k_0 and the hydrodynamic sound velocity shown in Fig. 1(d). The frequencies are given in cm^{-1} (1 cm^{-1}=0.03 THz=0.1885 ps^{-1}).

siderably better *quantitative* agreement between experimental and simulation data is obtained. In summary, the comparison of thermodynamic data indicates that the simulations are reliable regarding the qualitative trends in behavior, but good quantitative agreement is not found. Accordingly, we do not base any statements below that require strict quantitative agreement of simulation data with experimental results.

In Fig. 2, the static structure factor at five different temperatures are shown. Comparing these results with the experimentally measured structure factor at low k is by itself particularly important. From a small angle x-ray scattering study for $k>0.15$ Å^{-1}, Bosio et al.[18,19] estimated that density fluctuations with a length scale of 8 Å were present in supercooled water. A more recent study by Xie et al.[20] to lower k values ($k>0.05$ Å^{-1}) indicates that correlation lengths are considerably smaller than reported by Bosio et al., and furthermore, the variation with temperature is also small. Since this measurement has important implications to the understanding of supercooled behavior, a comparable MD study is very desirable. Indeed, no comparison between simulations and experiments have been ever performed due to the small k-vector required. Although performed at constant volume, the present simulations confirm that at high temperature, $S(k)$ is almost flat in the region below 0.4 Å^{-1} and that a very weak minimum in the static structure factor develops when the temperature is much smaller than the TMD value. Compared to the experimental data in Ref. 18, the minimum is much less pronounced. This difference could be due partially to the isochoric path of the simulated systems that produces an increase in pressure below the TMD and the associated decrease of the compressibility. While the data presented here are not accurate enough to make reliable estimates of the low k line shape and correlation lengths, a reliable estimate of the intercept at $k=0$ can be extracted and used to estimate the compressibility and the hydrodynamic sound speed.

IV. GENERAL OVERVIEW

Before entering a formal discussion of the k and ω behavior of longitudinal and transverse excitations, data at

one fixed small k value are presented to get a broad view of the physical processes occurring in the liquid. In the same spirit, the frequencies for characteristic molecular modes are mentioned.

Figure 3 shows the longitudinal and transverse component at different temperatures for $k=0.0536$ Å^{-1}, corresponding to a wavelength of about 120 Å. For J_l at each temperature, a vertical line denotes the peak position that would be expected, for the TIP4P potential, if no positive dispersion were present.

It is seen that on decreasing the temperature, the magnitude of the dispersion for the longitudinal mode (as indicated by the distance between the line and the peak) increases strongly. The transverse currents display behavior consistent with the longitudinal currents. The width of the $J_t(k,\omega)$ peak increases significantly on lowering the temperature and develops below 270 K into a peak centered at a nonzero frequency. Thus, even at a length scale of 120 Å, collective transverse excitations are observed in the simulation, indicating an elastic component in the generalized viscosity.

Figure 4 shows the dispersion relations obtained from the peak positions in $J_l(k,\omega)$. The velocities obtained from dividing the frequencies by the corresponding wave numbers are shown in Fig. 5. It is clear from these figures that a continuous change in velocities is observed in the studied range of k values, and the velocity values span a wide range, reaching values comparable to the hydrodynamic velocity at the smallest k values. Thus, the data presented in these figures offer very clear evidence that there is indeed only one propagating longitudinal mode, suggesting further that the origin of the high velocities observed is viscoelasticity. Experimentally, the longitudinal velocity measured using Brillouin scattering at -10 °C is found to be higher than the velocity obtained at ultrasonic frequencies,[21] corroborating the simulation results. From the velocities at lower k values [since they are higher than the
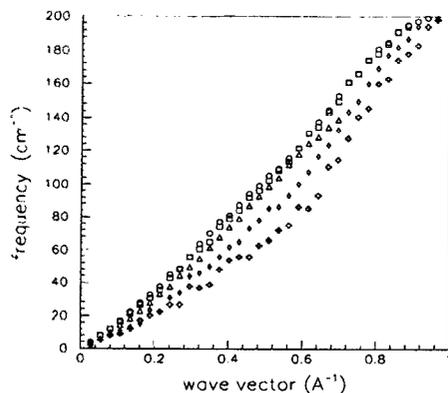
FIG. 4. Dispersion relations for longitudinal sound obtained from the peak position of $J_l(k,\omega)$ for $T=225$ (O); 240 ($\square$); 270 ($\triangle$); 320 ($\lozenge$); and 370 K (crosses). The same notation for the temperatures will be used in all the following pictures when data for different temperatures are shown together.

FIG. 6. Transverse current correlation functions $J_t(k,\omega)$ from the MD simulations (solid lines) for $T=240$ K. The fits obtained from Eqs. (5.1) and Eq. (5.3) are shown as dotted lines. $k_0=0.0268$ Å^{-1}.

hydrodynamic sound velocities shown in Fig. 1(d), especially for the lower temperatures], it may be inferred that positive dispersion has begun to occur at lower k values than the ones studied here. This, however, does not dilute the evidence presented, since positive dispersion continues well into the k regime studied. Thus, a viscoelastic analysis of the data is in order, which is taken up next.

It is also worth noting, in anticipation of the discussion in the following sections, that the frequency region shown in Fig. 3 is below the frequencies corresponding to the lowest ω peak in the density of states (DOS) (see, e.g., Figs. 12 and 13 in Ref. 22). This peak, centered ~ 60 cm^{-1}, is usually associated with the O–O–O bending modes.[23] It has also been interpreted (controversially) in terms of transverse acoustic modes propagating in hydrogen bonded patches of water molecules.[24,25] Higher ω peaks, centered at 180 and 250 cm^{-1}, have been associated with O–O stretching modes. These modes are the main "localized" modes that shall be of interest in the following discussion. Below 60 cm^{-1}, no interference between the acoustic modes (longitudinal and transverse) with local molecular modes of O–O–O bending or O–O stretching can be invoked to explain the positive dispersion previously discussed.

On the basis of the data reported in Figs. 3 and 4 and the considerations discussed, we try to apply viscoelastic theory to the data extracted from our simulations.

V. CURRENT CORRELATION FUNCTION—THE TRANSVERSE 0–50 cm^{-1}

Figures 6 and 7 show the transverse current function $J_t(k,\omega)$ for selected k vectors at two selected temperatures $T=240$ and 320 K (full lines). $J_t(t,\omega)$'s for k larger than a temperature dependent k value display a peak at finite frequency. The presence of such a peak is a clear indication of the propagation of shear waves in the medium. The dispersion relation for the transverse propagating modes is shown in Fig. 8. It is observed that at very low temperature, transverse modes exist down to the smallest k vector accessible in the present simulation. Thus, liquid water be-
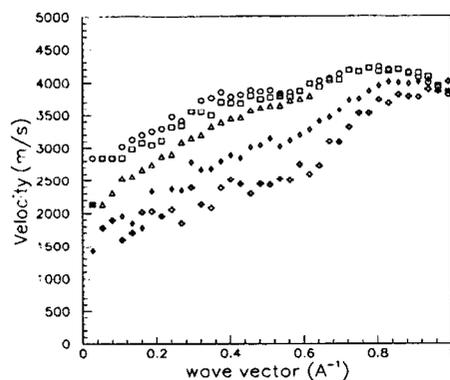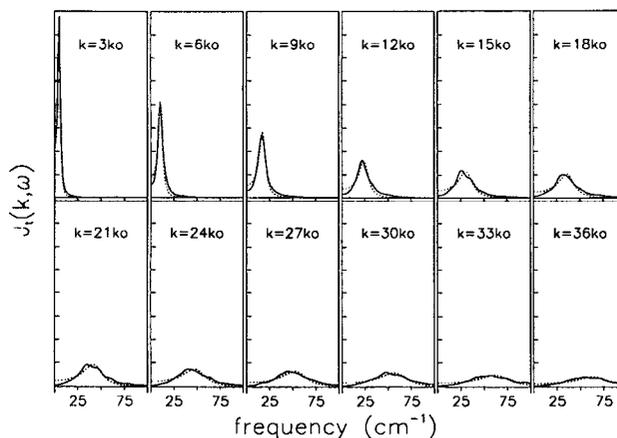

FIG. 5. Velocities obtained by dividing the peak frequency values in Fig. 4 by k. The velocities change continuously for all temperatures shown. Symbols are the same as in Fig. 4.
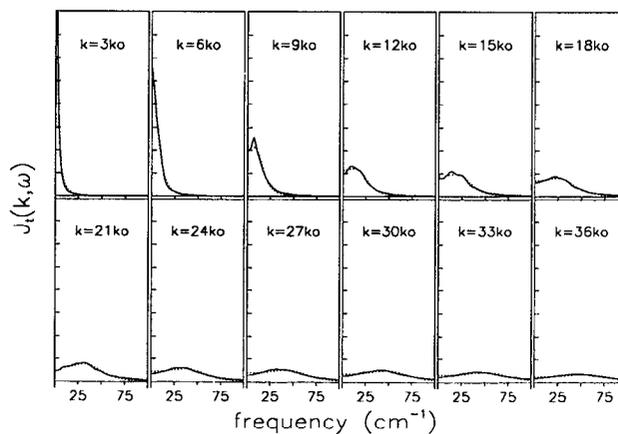

FIG. 7. Transverse current correlation functions $J_t(k,\omega)$ from the MD simulations (solid lines) for $T=320$ K. The fits obtained from Eqs. (5.1) and (5.3) are shown as dotted lines. $k_0=0.0268$ Å^{-1}.
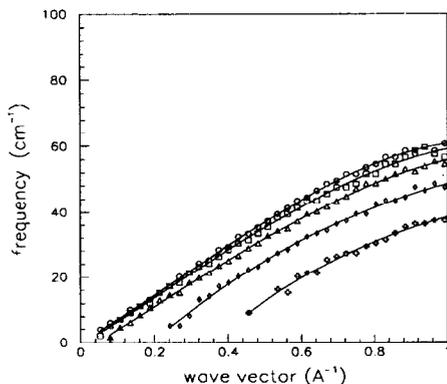
FIG. 8. The dispersion relations for the transverse sound modes at different temperatures. At high temperatures, no propagating mode exists at low k values. Symbols are the same as in Fig. 4.
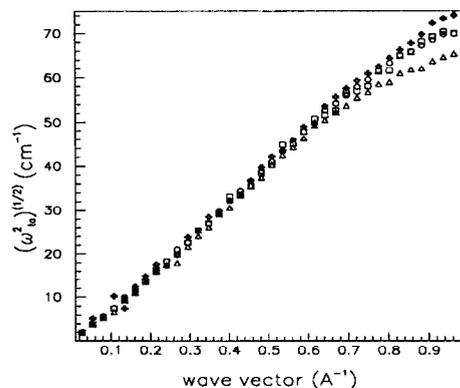

FIG. 9. Values of $\omega_{ta}(k)$ obtained from the fits of $J_t(k,\omega)$. Unlike the peak frequencies shown in Fig. 8, ω_{ta} values do not show appreciable change with temperature. Symbols are the same as in Fig. 4.

haves like a viscoelastic solid on length scales of 100 or more Å at low T (240 K). In experiments, the transverse mode is not seen even though $C_P \sim C_V$, making such an observation favorable. From our data, at the lowest T (which is 25° below the simulation TMD), the transverse peak appears for $k \sim 0.04$ Å^{-1}, which is a much larger k than is spanned in light scattering experiments. On increasing the temperature, the average length over which transverse excitations are able to propagate decreases, reaching about 10 Å at 370 K. The transverse velocity at small k, as measured from the slope of the dispersion relation, is found about 1300 m/s for all the temperatures, and decreases on increasing the wave vector. The value 1300 m/s for the transverse velocity is to be compared with the value 1900 m/s found in polycrystalline hexagonal ice for the propagation of transverse modes.[26] It is worth noting that the sound speed for the transverse acoustic branch calculated from simulations of ice I_h using TIP4P along the crystallographic directions (0001), (11$\bar{2}$0), and (01$\bar{1}$0) is very close to the experimental values.[27]

The observed behaviors of $J_t(k,t)$ and $v_t(k)$ are analyzed below in terms of generalized hydrodynamics. On going from the hydrodynamic limit to the finite k and ω regions, the kinematic viscosity coefficient ν, which in the hydrodynamic limit controls the damping of the nonpropagating transverse excitations, becomes a function of k and ω. Following the conventional treatment for normal liquids,[11] $J_t(k,\omega)$ in the acoustic region is expressed as

$$J_t(k,\omega) = 2v_0^2 \frac{k^2 K_t'(k,\omega)}{[\omega + k^2 K_t''(k,\omega)]^2 + [k^2 K_t'(k,\omega)]^2},$$
(5.1)

where the unknown k and ω dependence of the kinematic viscosity is transferred to the K' and K'' functions. The correct hydrodynamic limit is ensured by the condition

$$\lim_{\omega \to 0} \lim_{k \to 0} K_t'(k,\omega) = \nu.$$
(5.2)

It can be shown that K' and K'' are the real and imaginary parts of the memory function K that controls the evolution of $J_t(k,\omega)$. The simplest approximation for $K(k,t)$ is a single exponential decay

$$K(k,t) = K(k,0) \exp[-t/\tau_t(k)].$$
(5.3)

For atomic liquids, initial conditions require the $t=0$ value of the memory function to be

$$K(k,0) = \omega_{ta}^2(k)/k^4,$$
(5.4)

where $\omega_{ta}^2(k)$ is the second frequency moment of the current correlation function $J_t(k,\omega)$. In an atomic system, $\omega_{ta}(k)/k$ can be thought of as the velocity of propagation of transverse excitation if the damping due to viscosity is negligible ($\omega\tau \gg 1$). Roughly speaking, the finite frequency peak position is an indication of elastic behavior, while the distance between the peak position of the transverse excitation and $\omega_{ta}(k)$ is an indication of the presence of viscous effects.

In a molecular liquid, modes present at frequencies higher than the frequency range of the sound propagation contribute to the formal expression of the second frequency moment of the current correlation function. Thus, even to the extent that it is valid for atomic liquids, the one exponential functional form for the memory function K in Eq. (5.4) is not a good approximation for a molecular liquid. Hence, in the following discussion, we consider ω_{ta} as the normalized second frequency moment of the acoustic part of J_t and retain the subscript a on ω_{ta} as a reminder.

The numerically calculated J_t's are fitted to the above expression in the range 0–100 cm^{-1} by finding the least square minimum in the parameter space defined by τ_t and $K(k,t=0)$. The curves obtained by the fit are shown superimposed on the numerical data in Figs. 6 and 7. The quality of the fit is very good, even though there is room for further improvement.

The fitted values of $\omega_{ta}(k)$ and $\tau_t(k)$ are shown in Figs. 9 and 10. Note that the $\omega_{ta}(k)$ values at small k are temperature independent over a large k range. The velocity obtained from the slopes in Fig. 9 is ~ 1450 m/s, which has to be compared with the ~ 1900 m/s value observed in ice. The fact that the fitted $\omega_{ta}(k)$ values are temperature in-
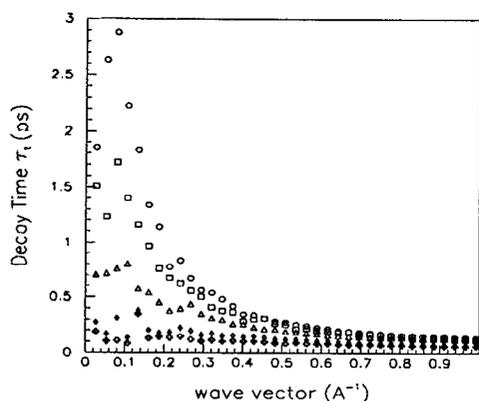
FIG. 10. Values of relaxation or decay times $\tau_t(k)$ obtained from fitting $J_t(k,\omega)$. The τ_t values increase on decreasing k and T. The continuous lines are drawn as a guide for the eye. Symbols are the same as in Fig. 4.

dependent strengthens the validity of the fit as well as the interpretation of $\omega_{ta}(k)/k$ in terms of the velocity of propagation of high frequency transverse excitations. The fitted values for $\tau_t(k)$ (which is a measure of the inverse width of J_t) are a decreasing function of k and T, in agreement with the interpretation of $\tau_t(k)$ as the lifetime of the collective excitation.[8]

Before concluding this section, we note that a better approximation for $K(k,t)$ is to express it in terms of two exponentials.[7,28] Such a form does indeed give better fits to the data and further avoids the need for treating the acoustic part of $J(k,\omega)$ separately. However, we find that very different sets of fitting parameters produce fits of the same quality. Hence, we prefer to present only the simpler and less ambiguous single exponential fit. We stress, however, that the single exponential approximation has to be considered as the first approximation to $K(k,t)$.

VI. LONGITUDINAL CURRENT CORRELATION FUNCTION

The description of longitudinal fluctuations in a liquid is more involved than that of transverse fluctuations. Even at the hydrodynamic level, the longitudinal modes are more complex than the transverse ones. *Ad hoc* assumptions are often needed to get a reasonable agreement between calculated and measured dynamic structure factors, even for simple liquids. As done for $J_t(k,\omega)$, $J_l(k,\omega)$ is also expressed in terms of the single exponential memory function to clarify the meaning of the computed quantities. Requiring the correct limit for the hydrodynamic regime and the correct sum rules, $J_l(k,\omega)$ can be written as

$$J_l(k,\omega) = v_0^2 \frac{\omega^2 k^2 D'(k,\omega)}{[\omega^2 - [(kv_0)^2/S(k)] + \omega k^2 D''(k,\omega)]^2 + [\omega k^2 D'(k,\omega)]^2},$$

(6.1)

where D' and D'' are functions which determine, respectively, the damping and dispersion in the longitudinal current fluctuations. The k and ω dependencies of the transport coefficient which controls J_l is transferred in the unknown D' and D'' functions. The simplest approximation for D' and D'' are derived from assuming a single exponential function for the shear relaxation mode. In this approximation, we have

$$D'(k,\omega) = \frac{(\gamma-1)v_0^2}{S(k)} + \frac{D_T k^2}{\omega^2 + (D_T k^2)^2} + \Phi_l(k,0) \frac{\tau_l(k)}{1+\omega^2\tau_l^2(k)}$$

(6.2)

and

$$D''(k,\omega) = -\frac{(\gamma-1)v_0^2}{S(k)} \frac{\omega}{\omega^2 + (D_T k^2)^2}$$
$$-\Phi_l(k,0) \frac{\omega\tau_l^2(k)}{1+\omega^2\tau_l^2(k)}$$

(6.3)

with

$$\Phi_l(k,0) = \frac{\omega_{la}^2(k)}{k^2} - \frac{\gamma v_0^2}{S(k)}.$$

(6.4)

Here, D_T is the thermal diffusivity, γ is the ratio of the specific heats, and $\omega_{la}^2(k)$ is the normalized second fre-

quency moment of the acoustic part of $J_l(k,\omega)$. ω_{la} is proportional to the high frequency elastic constant $c_{11}(k)$.[11]

The associated dispersion relation is given by

$$\omega^2 - \frac{(kv_0)^2}{S(k)} + \omega k^2 D''(k,\omega) = 0.$$

(6.5)

By standard algebra, this expression can be written in the limit $\omega > D_T k^2$ as

$$v_s(k)^2 = c_0(k)^2 + [c_\infty(k)^2 - c_0(k)^2]\frac{\omega^2\tau_l^2(k)}{[1+\omega^2\tau_l^2(k)]}$$

(6.6)

with

$$c_0(k)^2 = \frac{\gamma(kv_0)^2}{S(k)k^2}$$

(6.7)

and

$$c_\infty(k)^2 = \frac{w_{la}^2(k)}{k^2}.$$

(6.8)

Here, $c_0(k)$ is the generalization at finite k of the ordinary sound velocity and c_∞ is the high frequency sound speed. Again, c_∞ is the sound velocity that would be observed if the viscous contribution is negligible $(\omega\tau > 1)$.
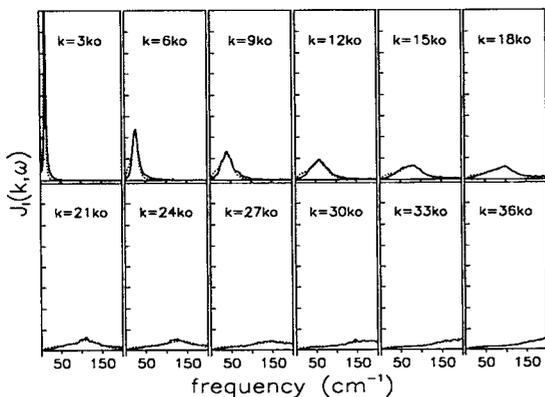
FIG. 11. Longitudinal current correlation functions $J_l(k,\omega)$ from the MD simulations (solid lines) for $T=240$ K. The fits obtained from Eqs. (6.1) and (6.4) are shown as dotted lines. $k_0=0.0268$ Å^{-1}.

FIG. 13. Values of $\omega_{la}(k)$ obtained from fitting $J_l(k,\omega)$. ω_{la} values do not show appreciable change with temperature except at high k. Symbols are the same as in Fig. 4.

The numerical data for J_l are fitted to the form described with ω_{la}^2 and τ_l as the fitting parameters. The fitted curves for J_l are shown superimposed on the numerical data in Figs. 11 and 12 for two temperatures $T=240$ and 320 K. The fitted values of $\omega_{la}(k)$ and $\tau_l(k)$ are shown in Figs. 13 and 14. It is seen that $\tau_l(k)$ increases as k decreases and further increases in amplitude as the temperature is lowered. This is well in accordance with the expected behavior. As in the case of the transverse current correlations, the value of ω_{la} from the fit is temperature independent in the small k range. At higher k, ω_{la} seems to become temperature dependent. This temperature dependence could reflect the differences between local structures of the liquid at different temperatures, differences which become amplified when k becomes comparable to the short range order, or it could be due to the breaking of the single exponential fit approximation.

From the data presented in the foregoing sections, it is seen that the viscoelastic approximation describes fairly adequately the behavior of both longitudinal and transverse sound propagation. It is seen that for the studied k values, which span a wide range of propagation velocities,
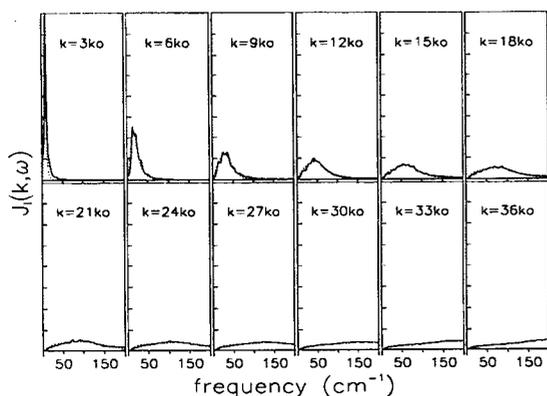
only one longitudinal sound mode is present. Furthermore, the $k\rightarrow 0$ limits of ω_{la}/k and ω_{ta}/k give satisfactory values for the high frequency sound velocity.

In the previous discussion, we have pointed out that ω_{la} and ω_{ta} are the second moments of the acoustic part of J_l and J_t. Indeed, in a molecular solid, J_l and J_t have contributions also from the presence of excitations different from the acoustic ones, i.e., from the localized ("optical") excitations. These modes, although they are characterized by a very low intensity, are amplified by the ω^2 factor on calculating the second moment and thus add their own contribution to the total ω_t^2 and ω_l^2 (see Appendix A). As a result, $\omega_l(k)/k$ and $\omega_t(k)/k$ cannot be thought of as velocities of propagation for the longitudinal and transverse acoustic modes, as in simple liquids, and have to be replaced in the first approximation (i.e., neglecting coupling between acoustic and other modes) by their acoustic part. For a molecular liquid with pair additive interactions, $\omega_t(k)$ and $\omega_l(k)$ are given in terms of the pair distribution functions $g_{\alpha\beta}(r)$ and the pair potentials $u_{\alpha\beta}(r)^6$ as

FIG. 12. Longitudinal current correlation functions $J_l(k,\omega)$ from the MD simulations (solid lines) for $T=320$ K. The fits obtained from Eqs. (6.1) and (6.4) are shown as dotted lines. $k_0=0.0268$ Å^{-1}.
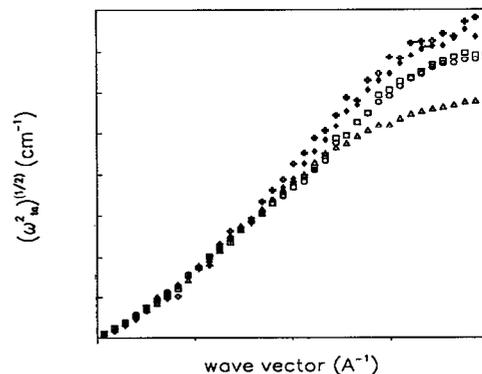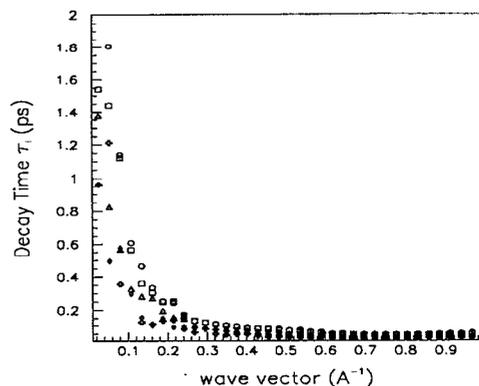

FIG. 14. Values of relaxation or decay times $\tau_l(k)$ obtained from fitting $J_l(k,\omega)$. The τ_l values increase on decreasing k and T. Symbols are the same as in Fig. 4.
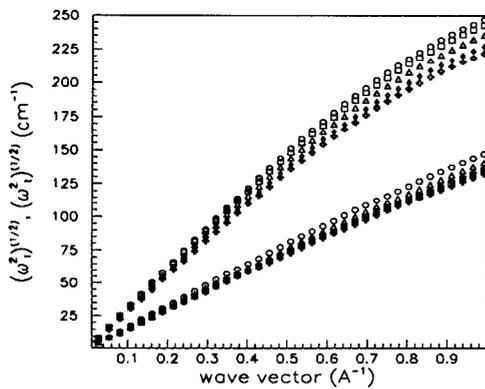
FIG. 15. $\omega_l(k)$ and $\omega_t(k)$ at different temperatures. Symbols for the different temperatures are the same as in Fig. 4.

$$\omega_l^2(k) = 3k^2 v_0^2 + \frac{n}{M} \sum_{\alpha\beta} \int d^3r\, g_{\alpha\beta}(r)$$

$$\times [\delta_{\alpha\beta} - \cos(kz)] \frac{\partial^2 u_{\alpha\beta}(r)}{\partial z^2} \qquad (6.9)$$

and

$$w_t^2(k) = k^2 v_0^2 + \frac{n}{M} \sum_{\alpha\beta} \int d^3r\, g_{\alpha\beta}(r)$$

$$\times \frac{[\delta_{\alpha\beta} - \cos(kz)]}{k^2} \frac{\partial^2 u_{\alpha\beta}(r)}{\partial x^2}. \qquad (6.10)$$

Here n is the number density, M is the molecular mass, v_0^2 is the thermal velocity ($v_0^2 = k_B T/M$), k_B is the Boltzmann's constant, and α and β indicate the interacting sites of the water molecule. In the TIP4P model potential, these are the positions of the three atoms and of the virtual site on the HOH angle bisector.

The ω_l^2 and ω_t^2 values, calculated according to the previous equations and shown in Fig. 15, are significantly larger than the ω_{la}^2 and ω_{ta}^2 values derived from the fit. Thus, care has to be taken in interpreting the significant positive sound speed dispersion in terms of ω_l^2 and ω_t^2.[6]

VII. NORMAL MODE ANALYSIS OF QUENCHED CONFIGURATIONS

Although the viscoelastic approximation seems to describe the overall behavior well, other effects have to be considered when studying molecular liquids and particularly associated liquids.[29] Indeed, in a previous paper,[5] we showed that in the region around $\omega \sim 60$ cm^{-1}, the longitudinal sound mode meets the k independent O–O–O bending mode.[5]

To study this issue further, we analyze the sound propagation via the technique of normal mode analysis of quenched configurations (described in Appendix B) with the aim of suppressing viscous effects without modifying the structure of the system. From the simulation of the liquid, a quenched configuration is obtained by an instantaneous quench, which is implemented by a rapid rescaling of the velocities or by a minimization of the potential en-

ergy starting with the coordinates of the initial liquid configuration in the $6N$ dimensional space of coordinates for a system of N molecules. Since the quenched configuration is a potential energy minimum, many standard techniques of normal mode analysis in solids can be applied to study the quenched system, although the simplifications arising from translational symmetry cannot be exploited.

The study of structural and dynamical properties of liquids through the study of quenched configurations or "inherent structures" is based on the following intuitive picture of the liquid state: The liquid at any instant resides in an approximately harmonic potential energy minimum (in configuration space) and the microscopic motion may roughly be described on short time scales as being oscillatory. Such oscillatory motion is periodically interrupted by jumps from one minimum of the potential energy hypersurface to another. Stillinger and Weber[30-32] tested this intuitive picture of liquid dynamics in simulations where quenched structures were obtained from successive configurations in a MD simulation of the liquid. The time evolution of the potential energy minimum values they found showed evidence for the phase point describing the system moving in the manner described above. On the basis of this simulation work, Zwanzig[33] formulated a simple argument for obtaining the diffusion constant and the velocity autocorrelation function in terms of the vibrational frequencies around the minima and hopping frequencies over barriers. More recently, calculations have been performed to relate the diffusive behavior in the liquid to the imaginary frequencies obtained in the normal mode analysis of instantaneous liquid configurations.[34,35] The study of quenched configurations has been applied to the case of water to study in detail the harmonic dynamics[31] and the local molecular structure.[36]

An attempt is made here to augment the approaches of using configurational information (as in Refs. 31 and 36) and the density of states (DOS) information (as in Refs. 34 and 35), by using in addition the normal modes as tools to study dynamics in the liquid state. In this spirit, we calculate the longitudinal current correlation function [for the center of mass (c.m.) coordinates] for an harmonic system. We denote the mth normal mode by t_m and the displacement of the lth molecule's c.m. along wave vector $\mathbf{k}$ for the mode m by $a(l,m)$. Then

$$\mathbf{k} \cdot \mathbf{r}_l(t) = k r_l(0) + k \sum_m \frac{a(l,m)}{M^{1/2}} t_m, \qquad (7.1)$$

where $r_l(0)$ is the equilibrium c.m. position of the molecule l, and $M^{1/2}$ in the second term accounts for the fact that $a(l,m)$'s are normalized coordinates. Similarly, we write

$$\frac{\mathbf{k}}{k} \cdot \mathbf{v}_l(t) = \sum_m \frac{a(l,m)}{M^{1/2}} \dot{t}_m. \qquad (7.2)$$

Substituting the above expressions in Eq. (2.4), we obtain

$$j_k(t) = \frac{1}{N^{1/2}} \sum_l \sum_m \frac{a(l,m)}{M^{1/2}} \dot{t}_m(t)$$

$$\times \exp\left\{ ik\left[r_l(0) + \sum_n \frac{a(l,n)}{M^{1/2}} t_n(t) \right] \right\}. \qquad (7.3)$$

The longitudinal current correlation function $J_l(k,t)$ $\equiv \langle j_k(0) j_k^*(t) \rangle$ is then given by

$$J_l(k,t) = \frac{1}{NM} \sum_l \sum_{l'} \sum_m \sum_{m'} \{\exp ik[r_l(0) - r_{l'}(0)]\}$$

$$\times a(l,m) a(l',m') \left\langle \dot{t}_m \dot{t}_{m'}(t) \right.$$

$$\times \exp\left[ik \sum_n \frac{[a(l,n)t_n - a(l',n)t_n(t)]}{M^{1/2}} \right] \right\rangle. \qquad (7.4)$$

Since the Hamiltonian of the system $\mathcal{H} = \Sigma_m \frac{1}{2}\omega_m^2 t_m^2 + \frac{1}{2}\dot{t}_m^2$ is quadratic in t_m and $\dot{t}_m$, we have,

$$\left\langle \dot{t}_m \dot{t}_{m'} \exp\left[ik \sum_n a(l,n)t_n - a(l',n)t_n \right] \right\rangle = \langle \dot{t}_m \dot{t}_{m'} \rangle$$

$$\times \left\langle \exp\left\{ ik \sum_n \frac{[a(l,n)t_n - a(l',n)t_n(t)]}{M^{1/2}} \right\} \right\rangle, \qquad (7.5)$$

$$\langle \dot{t}_m \dot{t}_{m'} \rangle = \delta_{mm'} \beta^{-1} \cos(\omega_m t), \qquad (7.6)$$

and

$$\left\langle \exp\left[ik \sum_n a(l,n)t_n - a(l',n)t_n(t) \right] \right\rangle$$

$$= \exp\left\{ -\sum_n \frac{k^2}{2M\beta\omega_n} [a(l,n)t_n - a(l',n)t_n(t)]^2 \right\}. \qquad (7.7)$$

Here, β is the inverse temperature, and the time dependence of t_m is shown explicitly only in the expression for $\langle \dot{t}_m \dot{t}_{m'} \rangle$. The Fourier transform of $J_l(k,t)$ in the low temperature of one-phonon approximation (which corresponds to setting $\exp\{-\Sigma_n[k^2/(2M\beta\omega_n)][a(l,n)t_n -a(l',n)t_n(t)]^2\}$ to 1) is then given by

FIG. 17. The dispersion relation for the quenched configuration obtained from the peak positions of $J_l(k,\omega)$ in Fig. 16.

$$J_l(k,\omega_m) = \frac{v_0^2}{N} \sum_l \sum_{l'} a(l,m) a(l',m)$$

$$\times \exp\{ik[r_l(0) - r_{l'}(0)]\}. \qquad (7.8)$$

$J_l(k,\omega)$ obtained by this procedure are shown in Fig. 16. From the peak positions of J_l, one may obtain the dispersion relation for the quenched system. This is shown in Fig. 17. We see that there is significant dispersion in the frequency range of 50–100 cm^{-1} for the quenched system. Moreover, the system being elastic the dispersion in Fig. 17 is due completely to structural effects and cannot be attributed to the transition from viscous to elastic behavior.

In order to obtain some indication of qualitative difference between oscillations below and above the frequency range under investigation, the normal mode analysis is carried out disregarding the off-diagonal blocks of the Hessian matrix. These blocks contain terms coupling the c.m. and rotational coordinates. The full DOS and the DOS obtained for c.m. coordinates neglecting their coupling to rotational coordinates are compared in Fig. 18. The significant feature seen is that while below $\omega \sim 100$ cm^{-1} the c.m. frequencies show a considerable shift to higher values, a very small shift is seen above this frequency range. This
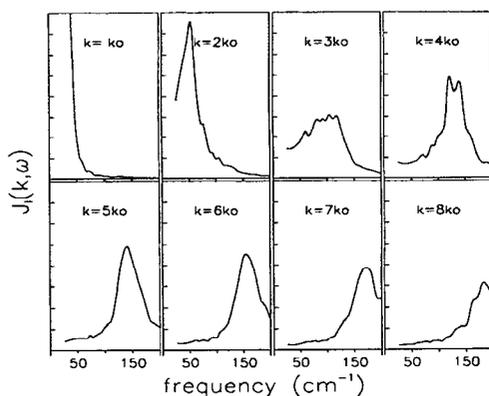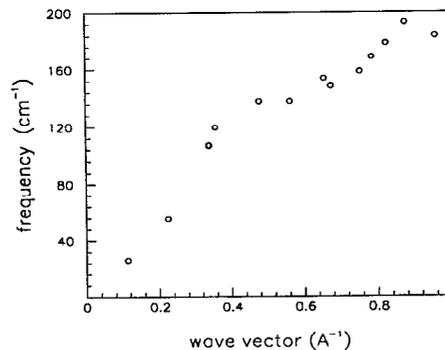

FIG. 16. $J_l(k,\omega)$ obtained from the normal modes of the quenched configuration. $J_l(k,\omega)$ obtained this way changes with T only by the Debye–Waller factor. $k_0 = 0.112$ Å^{-1}.
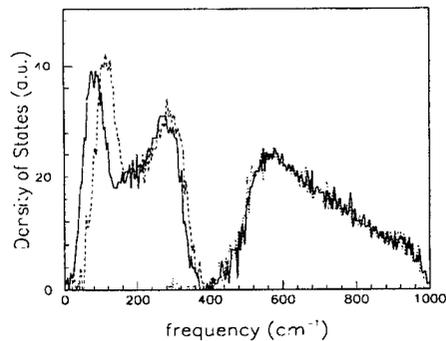

FIG. 18. Density of states obtained from the quenched configurations by normal mode analysis. The full lines are from diagonalizing the entire Hessian matrix [see Eq. (B2)]. The dotted line below 400 cm^{-1} is from diagonalizing the block containing center of mass coordinates only. The dotted line mostly above 400 cm^{-1} is from diagonalizing the block containing the rotational coordinates only.
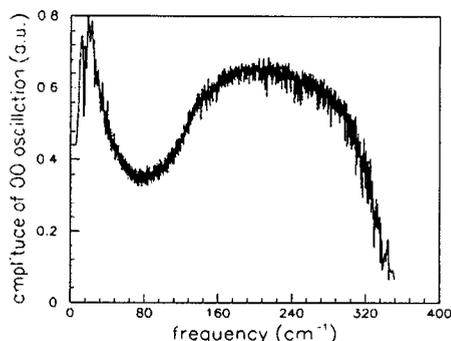
FIG. 19. The average amplitude of O–O stretching motion in the quenched system. Note the pronounced dip in the 50–100 cm^{-1} range.

indicates that while the modes in the frequency range below $\omega \sim 100$ cm^{-1} couple c.m. and rotational degrees of freedom significantly, modes above this range are purely c.m. modes. Thus, modes in the region commonly ascribed to the O–O–O bending are softened significantly by the coupling with rotational modes. Also shown in Fig. 18 is the DOS obtained by diagonalizing only the block containing rotational coordinates. It is seen that the frequencies obtained from this block are almost all in the range above 400 cm^{-1} and that there is no change in the DOS compared to the full diagonalization.

To further support this observation we show in Fig. 19 the amplitude of oscillations along the nearest neighbor oxygen–oxygen line for each mode, averaged over all the nearest neighbor oxygen–oxygen pairs. The averaging is done by exciting each mode with an energy of $\frac{1}{2}kT$. The nearest neighbors are clearly defined for a quenched configuration since the first minimum in the radial distribution function is very sharply defined.[32,36] We clearly see that the O–O stretching amplitude has a dip in the region between 50 and 100 cm^{-1}.

Results shown in Figs. 18 and 19 suggest that while the collective excitations in liquid water at very small frequencies (hydrodynamic region) are due predominantly to c.m. motion, between 50 and 100 cm^{-1} there is a significant mixing with the rotational (O–O–O bending) modes. The purely translational (stretching) character is restored above 100 cm^{-1}. This mixing is revealed in the dispersion relations as additional dispersion, independent of the one caused by viscoelastic effects.

VIII. CONCLUSIONS

In summary, the MD and normal mode analysis studies presented in this paper lead to the following conclusions:

(a) Below 50 cm^{-1}, the sound propagation in water can be described adequately by formal viscoelastic analysis. This conclusion is supported by the following:

(i) the direct observation of positive dispersion for the longitudinal sound (such a direct observation is made possible, for the first time, by the large simulated system size);

(ii) the temperature dependence of such a dispersion (at the smallest studied k vector, the sound velocity rise, compared to the hydrodynamic value, is a decreasing function of the temperature);

(iii) the existence of propagating transverse modes and by their k and T dependence;

(iv) the agreement between calculated and theoretical expressions for the longitudinal and transverse currents (we stress that the one exponential expression used to compare theoretical predictions and calculated data has to be considered a first order approximation).

(b) Between 50 and 100 cm^{-1}, the "interference" of the O–O–O bending mode in the frequency range of ~ 50–100 cm^{-1} leads to new interesting features in the longitudinal sound dispersion. Such features are superimposed on the viscoelastic behavior. We expect such behavior to be characteristic of molecular liquids, in particular, associated liquids. Other molecular liquids whose crystalline states display intersecting acoustic and optical branches may exhibit similar behavior. However, further study is necessary to obtain a better understanding of this phenomenon in water and to clarify the role of the network topology in influencing the propagation of sound in the frequency range, where the intersection of the acoustic and the bending mode takes place. We expect that a more detailed study of the sound propagation in quenched structures produced by quenching the liquid from different temperatures could furnish new interesting results.

(c) Only one collective acoustic excitation is present at each k. The sound speed moves from the hydrodynamic value to the large k value due mainly to the transition from viscous behavior to elastic behavior. The sound mode can be observed at large k (Ref. 1) since the normal sound attenuation is diminished on passing from the viscous to the elastic regime.

No clear connection to the hydrogen bond network emerges from this study, while the specific details of molecular excitations seem to play a significant role. While strong evidence against a novel excitation propagating on the hydrogen bond network is obtained, the role of the network topology in influencing the propagation of the single sound branch remains to be delineated with clarity.

ACKNOWLEDGMENTS

APPENDIX A

In this section, we derive the expression for ω_l^2 for an harmonic system. We then calculate ω_l^2 for a simple quasi-

two dimensional system to show the presence of optical contributions to ω_l^2. Analogous results can be obtained for ω_t^2.

Starting from the frequency sum rules for J_l, it is easy to show that for a system of N molecules of mass M (see Ref. 11)

$$\omega_l^2(k) = 3k^2v_0^2 + \frac{1}{MN}\sum_{ll'}\left\langle\frac{\partial^2 U}{\partial z_l \partial z_{l'}}e^{ikz_{ll'}}\right\rangle. \tag{A1}$$

Here U is the total potential energy and $z_{ll'}$ is the distance along z between the c.m. of molecules l and l'. In the normal mode representation, indicating the ith eigenvector with t_i, its eigenvalue with ω_i and the displacement of the c.m. of the molecule l along the z direction in the eigenmode i with $a(i,l)$, we have

$$U = \frac{1}{2}\sum_i \omega_i^2 t_i^2, \tag{A2}$$

$$\frac{\partial^2 U}{\partial z_l \partial z_{l'}} = \sum_i \omega_i^2 a(i,l)a(i,l')M, \tag{A3}$$

and

$$e^{ikz_{ll'}} = e^{ikz_{ll'}(0)}\exp\left[ik\sum_j[a(j,l)-a(j,l')t_j]/\sqrt{M}\right]. \tag{A4}$$

By performing the thermodynamic average over the normal modes t_i (which in an harmonic system is equivalent to calculating averages over a Gaussian distribution function), one obtains the exact expression

$$\omega_l^2(k) = 3k^2v_0^2 + \frac{1}{N}\sum_i\sum_{ll'}\omega_i^2 a(i,l)a(i,l')e^{ikz_{ll'}(0)}$$

$$\times\exp\left\{-k^2\frac{\sum_j[a(j,l)-a(j,l')]^2}{2M\beta\omega_j^2}\right\}. \tag{A5}$$

The configurational contribution to $\omega_l^2(k)$ (the second term in the previous expression) is thus written as a sum over all the normal modes. If a clear separation among acoustic, optical, and librational modes exists, $\omega_l^2(k)$ can also be separated in its acoustic, optical, and librational contributions. The acoustic part of $\omega_l(k)$ will retain the relation with the sound propagation as observed in simple liquids.

In the limit of $T\to 0$, the exponential at the end of the above expression is equal to one. In this limit, the meaning of ω_l^2 as the normalized second moment of $J_l(k,\omega)$, as given in Eq. (7.8) becomes evident.

Next we calculate ω_l^2 for a simple harmonic system composed of water molecules interacting via the TIP4P potential. We study a periodic two dimensional chain composed of 40 water molecules arranged in such a way that each water molecule participates in two hydrogen bonds, such that there are two molecules in the unit cell. A slight positional disorder introduced in the starting configuration is preserved by the minimization procedure. This system shows three well-resolved branches—an acoustic branch (below 50 cm^{-1}), an optical branch (between 150 and 300 cm^{-1}), and a librational band.
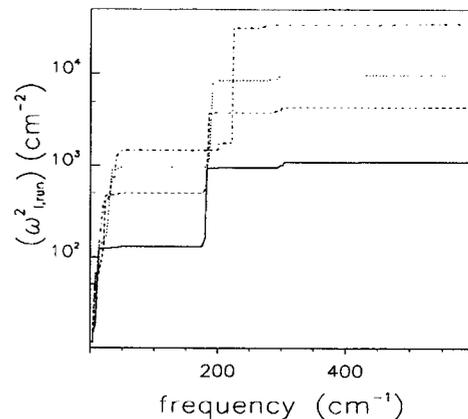

FIG. 20. Running integration of $\omega^2 J_l(k,\omega)$ calculated for a harmonic two dimensional chain of water molecules. The four smallest k vectors are shown. The limiting value of $\omega_{l,\text{running}}^2$ for $\omega\to\infty$ is ω_l^2.

Figure 20 shows, for the four smallest k vectors, the running integration of $\omega^2 J_l(k,\omega)$ [$\omega_{l,\text{run}}^2(\omega)$], i.e., the contribution to $\omega_l^2(k)$ of all the modes with frequency less than a prefixed ω value. From Fig. 20, we clearly see that both the acoustic and optical modes contribute to $\omega^2(k)$. Above the acoustic branch, $\omega_{l,\text{run}}^2(w)$ reaches a plateau which gives the acoustic contribution to ω_l^2, namely, ω_{la}^2. Only when the running argument ω has crossed the optical branch completely does $\omega_{l,\text{run}}^2(w)$ coincide with the second moment of $J_l(k,\omega)$. ω_{la}^2/k coincides with the longitudinal sound velocity of the chain. In such a simple system, where the acoustic and the optical branches are clearly separated, ω_l^2 can be separated into contributions arising from the acoustic and optical branches.

APPENDIX B

In this appendix, we describe briefly the procedure for obtaining the normal modes. Such procedure has been applied to a system of 634 water molecules interacting with a TIP4P potential.

Starting from an equilibrated liquid configuration, the closest potential energy minimum configuration is obtained by a steepest descents procedure. For the configuration obtained, we can expand the potential energy as

$$V(x_i\cdots x_N) = V(x_{0i}\cdots x_{0N}) + \frac{1}{2}\left(\frac{\partial^2 V}{\partial x_i \partial x_j}\right)_0 x_i x_j + \cdots, \tag{B1}$$

where the subscript 0 refers to the minimum positions of all the coordinates x_i. To obtain the normal modes, one diagonalizes the Hessian matrix of second derivatives

$$\mathscr{H}_{ij} = \left(\frac{\partial^2 V}{\partial x_i \partial x_j}\right)_0. \tag{B2}$$

For the present calculations, the Hessian matrix is defined for the set of $6N$ coordinates of the N water molecules, with $3N$ of the coordinates being center of mass

coordinates and $3N$ coordinates being rotational coordinates. In the expression above, the coordinates x_i are given in terms of actual coordinates as follows:

$$x_{i\alpha}^{c.m.} = (M)^{(1/2)} R_{i\alpha} \tag{B3}$$

for center of mass coordinates, where $R_{i\alpha}$ is the αth component of the c.m. position of the ith molecule with respect to its equilibrium position. Similarly,

$$x_{i\alpha}^{rot} = (I_\alpha)^{(1/2)} X_{i\alpha} \tag{B4}$$

for rotational coordinates, where $X_{i\alpha}$ is the angular position with respect to the αth principal axis and I_α is the momentum of inertia for that principal axis. The principal axes for the TIP4P water molecule are (i) perpendicular to the plane of the molecule; (ii) the bisector of the H–O–H angle; and (iii) the axis perpendicular to the first two. The Hessian matrix is calculated numerically by making small displacements along each of the coordinates. The matrix thus obtained is diagonalized using a standard numerical diagonalization package.

The Hessian matrix is composed of four large blocks. One block contains only c.m. coordinates and thus describes dynamics arising from purely c.m. interactions. The other block contains only rotational coordinates, while the last two blocks describe the coupling between c.m. and rotational coordinates.

[1] J. Teixeira, M.-C. Bellissent-Funel, S.-H. Chen, and B. Dorner, Phys. Rev. Lett. **54**, 2681 (1985).

[2] M. Wojcik and E. Clementi, J. Chem. Phys. **85**, 6085 (1986).

[3] M. A. Ricci, D. Rocca, G. Ruocco, and R. Vallauri, Phys. Rev. A **40**, 7226 (1989).

[4] Th. Kowall, P. Mausbach, and A. Geiger, Ber. Bunsenges. Phys. Chem. **94**, 279 (1990).

[5] S. Sastry, F. Sciortino, and H. E. Stanley, J. Chem. Phys. **95**, 7775 (1991).

[6] U. Balucani, G. Ruocco, A. Torcini, and R. Vallauri, Phys. Rev. E **47**, 1677 (1993).

[7] U. Balucani, G. Ruocco, M. Sampoli, A. Torcini, and R. Vallauri, Chem. Phys. Lett. **209**, 408 (1993).

[8] A. Rahman and F. H. Stillinger, Phys. Rev. A **20**, 368 (1974). The ST2 potential is defined in Ref. 22.

[9] R. W. Impey, P. A. Madden, and E. R. McDonald, Mol. Phys. **46**, 513 (1982).

[10] The TIP4P potential is defined in W. L. Jorgensen, J. Chandrasekhar, J. D. Madura, R. W. Impey, and M. L. J. Klein, Chem. Phys. **79**, 926 (1983).

[11] J. P. Boon and S. Yip, *Molecular Hydrodynamics* (McGraw–Hill, New York, 1980).

[12] J. P. Hansen and I. R. McDonald, *Theory of Simple Liquids* (Academic, London, 1986).

[13] W. H. Press, B. P. Flannery, S. A. Teukolsky, and W. T. Vetterling, *Numerical Recipes* (Cambridge, University, Cambridge, MA, 1988).

[14] L. Haar, J. S. Gallagher and G. Kell, *NBS/NRC Steam Tables* (Hemisphere, Washington, D.C., 1985).

[15] H. E. Stanley and J. Teixeira, J. Chem. Phys. **73**, 3404 (1980).

[16] M. P. Allen and D. J. Tildesley, *Computer Simulation of Liquids* (Oxford University, Oxford, 1989).

[17] P. H. Poole, F. Sciortino, U. Essmann, and H. E. Stanley, Nature **360**, 324 (1992).

[18] L. Bosio, J. Teixeira, and H. E. Stanley, Phys. Rev. Lett. **46**, 597 (1981).

[19] L. Bosio, J. Teixeira, and M.-C. Bellissent-Funel, Phys. Rev. A **39**, 6612 (1989).

[20] Y. Xie, K. F. Ludwig, Jr., G. Morales, D. E. Hare, and C. M. Sorensen, Phys. Rev. Lett. **71**, 2050 (1993).

[21] G. Maisano, P. Migliardo, F. Aliotta, C. Vasi, and F. Wanderlingh, Phys. Rev. Lett. **52**, 1025 (1984).

[22] F. H. Stillinger and A. Rahman, J. Chem. Phys. **60**, 1545 (1974).

[23] G. E. Walrafen, in *Water: A Comprehensive Treatise*, edited by F. Frands (Plenum, New York, 1972), Vol. 1.

[24] G. E. Walrafen, J. Phys. Chem. **94**, 2237 (1990).

[25] M. A. Ricci, G. Ruocco, and M. Sampoli, Mol. Phys. **67**, 19 (1989).

[26] R.E. Gagnon, H. K. Kiefte, and M. J. Clouter, J. Chem. Phys. **92**, 1909 (1990).

[27] F. Sciortino (unpublished results).

[28] D. Levesque, L. Verlet, and J. Kurkijarvi, Phys. Rev. A **7**, 1690 (1973).

[29] J. Alonso, F. J. Bermejo, M. Garcia-Hernandez, J. L. Martinez, W. S. Howells, and A. Criado, J. Chem. Phys. **96**, 7696 (1992); A Criado, F. J. Bermejo, M. Garcia-Hernandez, and J. L. Martinez, Phys. Rev. E **47**, 3516 (1993).

[30] F. H. Stillinger and T. A. Weber, Phys. Rev. A **25**, 978 (1982).

[31] F. H. Stillinger and T. A. Weber, J. Phys. Chem. **87**, 2833 (1983).

[32] T. A. Weber and F. H. Stillinger, J. Chem. Phys. **80**, 2742 (1984).

[33] R. Zwanzig, J. Chem. Phys. **79**, 4507 (1983).

[34] B. Madan, T. Keyes, and G. Seeley, J. Chem. Phys. **92**, 7565 (1990).

[35] B. Madan, T. Keyes, and G. Seeley, J. Chem. Phys. **94**, 6762 (1991).

[36] F. Sciortino, A. Geiger, and H. E. Stanley, Phys. Rev. Lett. **65**, 3452 (1990).